Electronic Supplementary Material (ESI) for RSC Advances.

Supporting Information

The Impact of Phenyl-Phenyl Linkage on the Thermodynamic, Optical and Morphological Behavior of Carbazol Derivatives

José C. S. Costa,*[ab] Marco A. L. Lima [a], Adélio Mendes [b], and Luís M. N. B. F. Santos *[a]

[a]*CIQUP, Centro de Investigação em Química da Universidade do Porto, Department of Chemistry and Biochemistry, Faculty of Science, University of Porto, Portugal. E-mail: jose.costa@fc.up.pt, lbsantos@fc.up.pt*

[b]*LEPABE, Laboratory for Process Engineering, Environment, Biotechnology and Energy, Faculty of Engineering, University of Porto, Portugal.*

Index

1. UV-Vis Absorption Spectroscopy

UV-vis absorption properties of mCP, CBP and TCB were explored using a diode array spectrophotometer (Agilent 8543 UV-visible spectroscopy system). Absorption spectra in diluted solutions (≈ 10^{-5} mol·dm^{-3}) using CH_2Cl_2 as a solvent were recorded over the range 200-700 nm, using quartz cells with a path length of 10.00 mm maintained at a constant temperature of T = 298.15 K. The detailed UV-Vis spectra for mCP, CBP and TCB are depicted in Figures S1-S3.

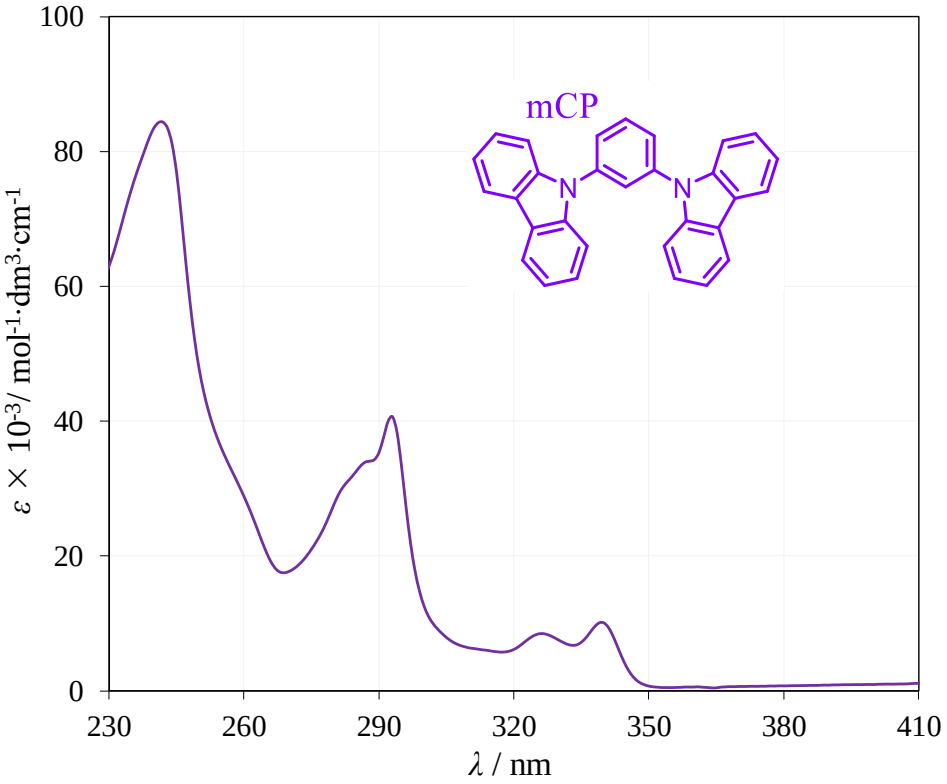

Fig. S1 UV-Vis spectrum of mCP recorded in CH_2Cl_2 at T = 298.1 K.

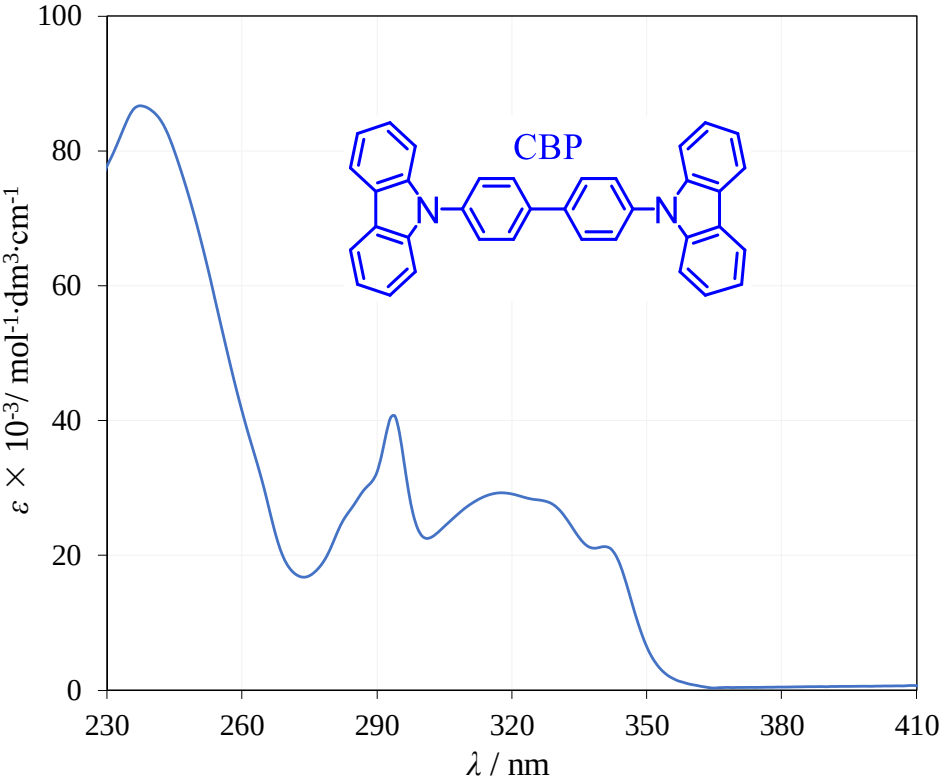

Fig. S2 UV-Vis spectrum of CBP recorded in CH_2Cl_2 at T = 298.1 K.

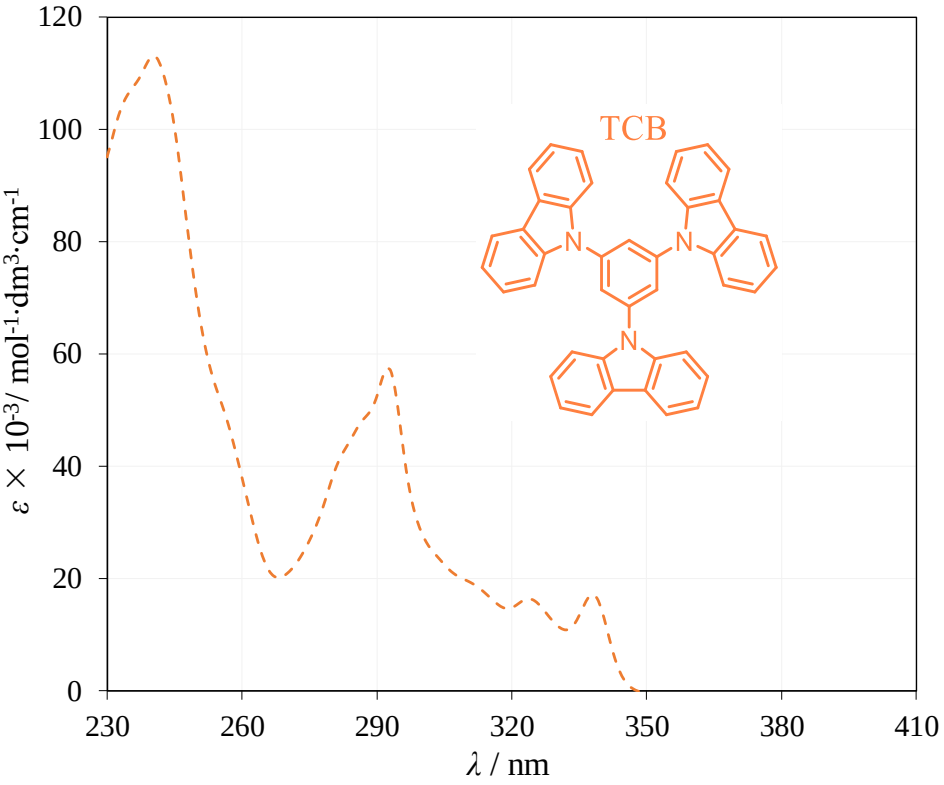

Fig. S3 UV-Vis spectrum of TCB recorded in CH_2Cl_2 at T = 298.1 K.

2. Differential Scanning Calorimetry

The melting temperatures and the thermodynamic properties of fusion for the compounds studied were determined in a heat flux differential scanning calorimeter (NETZSCH, DSC 200 F3) using a heating rate of 2 K·min^{-1}. The temperature and heat flux scales of the thermograms were calibrated (equations S1 and S2) measuring the temperature and enthalpy of fusion of some reference materials for thermal analysis: *o*-terphenyl, benzoic acid, indium, triphenylene, tin, perylene, and zinc.[S1, S2] The compounds studied were measured with the same experimental procedure used in the calibration runs. Standard molar enthalpies and entropies of fusion were calculated according to equations S3 and S4. The experimental results of mCP, CBP, and TCB are presented in Tables S1-S3. Typical DSC thermograms for the compounds studied are depicted in Figures S4-S7.

Temperature calibration, $T_m = 1.001284 \times T_{onset} - 1.036902$ (S1)

Energy calibration, $K = -0.0035398 \times T_m + 5.1914530$ (S2)

$$\Delta_{fus}H^{o} = \frac{A \times M}{m \times K} \quad \text{(S3)}$$

$$\Delta_{fus}S^{o} = \frac{\Delta_{fus}H^{o}}{T_m} \quad \text{(S4)}$$

Table S1 Experimental temperature and the standard molar enthalpy and entropy of fusion of mCP (M = 408.49 g·mol^{-1}).

m / mg	T_{onset} / K	A / μV·s	T_m / K	K / μV·s·mJ^{-1}	$\Delta_{fus}H^o$ / kJ·mol^{-1}	$\Delta_{fus}S^o$ / J·K^{-1}·mol^{-1}
5.91	454.1	1384	453.7	3.59	26.7	58.9
8.05	454.2	1966	453.8	3.59	27.8	61.3
8.98	454.2	2143	453.8	3.59	27.2	59.9
4.89	454.3	1153	453.9	3.58	26.9	59.2
			453.8 ± 0.2		**27.1 ± 1.4**	**59.8 ± 2.5**

Table S2 Experimental temperature and the standard molar enthalpy and entropy of fusion of CBP (M = 484.59 g·mol^{-1}).

M / mg	T_{onset} / K	A / μV·s	T_m / K	K / μV·s·mJ^{-1}	$\Delta_{fus}H^o$ / kJ·mol^{-1}	$\Delta_{fus}S^o$ / J·K^{-1}·mol^{-1}
5.45	554.24	1595	553.9	3.23	43.9	79.3
5.42	552.91	1569	552.6	3.24	43.4	78.5
3.31	554.28	949	554.0	3.23	43.0	77.7
3.93	554.30	1127	554.0	3.23	43.0	77.6
3.28	553.30	892	553.0	3.23	40.8	73.8
3.90	553.31	1100	553.0	3.23	42.3	76.4
3.21	554.27	915	553.9	3.23	42.7	77.1
			553.5 ± 1.2		**42.7 ± 2.8**	**77.2 ± 4.1**

Table S3 Experimental temperature and the standard molar enthalpy and entropy of fusion of TCB (M = 573.68 g·mol^{-1}).

m / mg	T_{onset} / K	A / μV·s	T_m / K	K / μV·s·mJ^{-1}	$\Delta_{fus}H^o$ / kJ·mol^{-1}	$\Delta_{fus}S^o$ / J·K^{-1}·mol^{-1}
3.60	324.5	806.	597.3	3.08	41.7	69.8
3.27	323.9	717	596.7	3.08	40.9	68.6
3.79	325.1	863	598.0	3.07	42.5	71.1
3.48	325.2	781	598.0	3.07	41.8	69.9
			597.5 ± 1.2		**41.7 ± 2.5**	**69.9± 4.2**

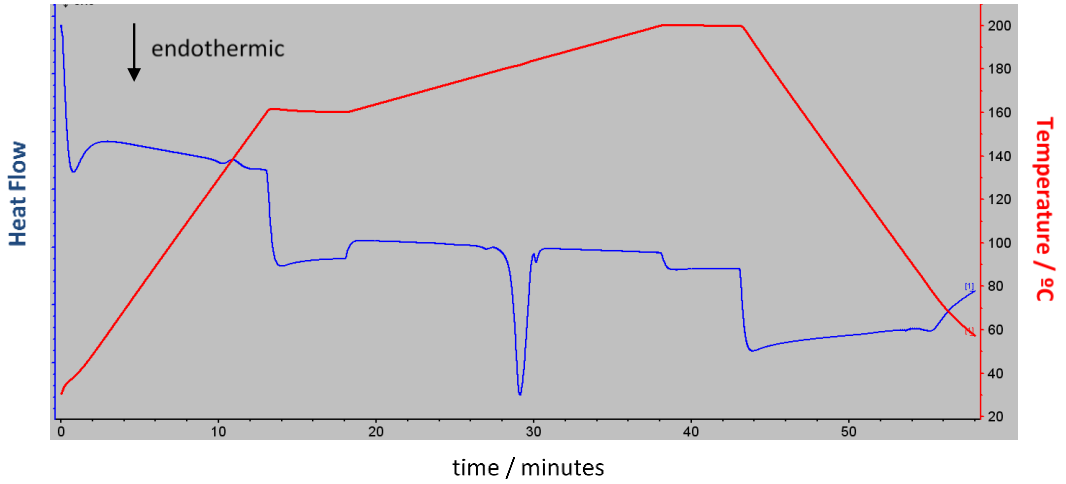

Fig. S4 Typical DSC thermogram for mCP applying a constant flow of nitrogen (50 $cm^3 \cdot min^{-1}$), a heating rate of 2 $K \cdot min^{-1}$ and using hermetically sealed aluminium crucibles (25 µl).

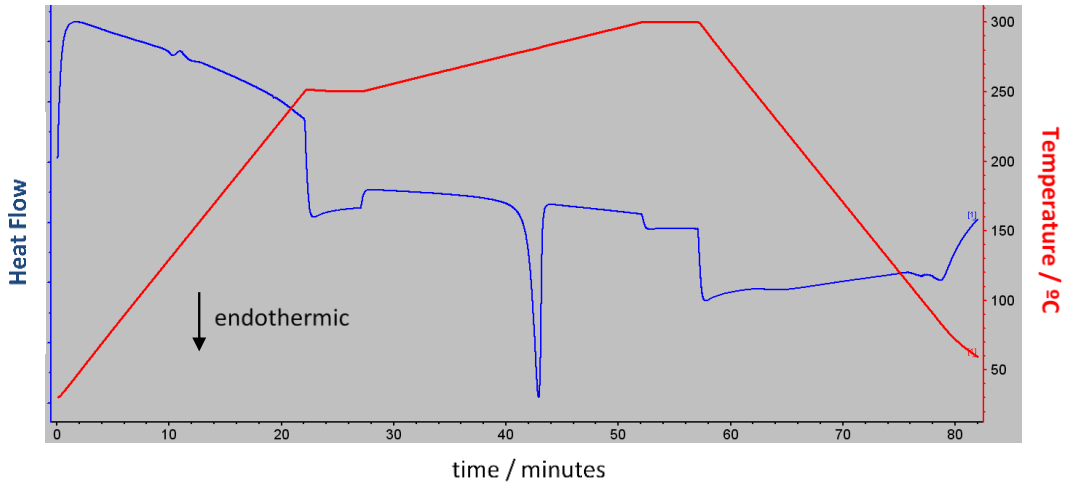

Fig. S5 Typical DSC thermogram for CBP applying a constant flow of nitrogen (50 $cm^3 \cdot min^{-1}$), a heating rate of 2 $K \cdot min^{-1}$ and using hermetically sealed aluminium crucibles (25 µl).

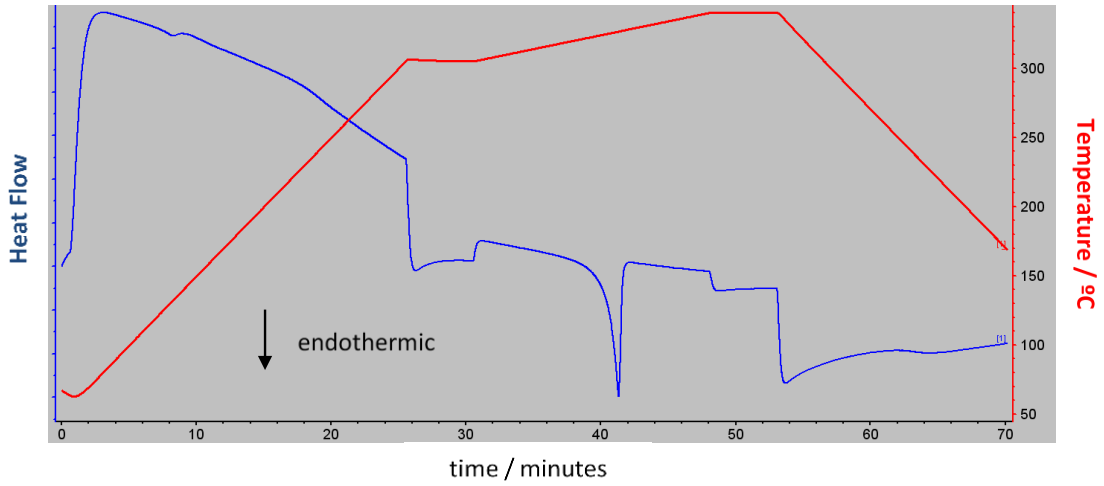

Fig. S6 Typical DSC thermogram for TCB applying a constant flow of nitrogen (50 $cm^3 \cdot min^{-1}$), a heating rate of 2 $K \cdot min^{-1}$ and using hermetically sealed aluminium crucibles (25 µl).

3. Knudsen Effusion & Vapor Pressure Measurements

Vapor pressures and thermodynamic properties of phase transition were determined through Knudsen effusion[S3-S6] for mCP, CBP, and TCB. The performance and accuracy of the Knudsen effusion approach was evaluated by measuring the equilibrium vapor pressures of 1,3,5-triphenylbenzene, an established reference organic compound for the enthalpy of sublimation and a recommended compound for sublimation studies at relatively high temperatures.[S1-S9] The equilibrium vapor pressures, p, of the compounds studied at various temperatures were determined through the Knudsen equation:

$$p = \frac{\Delta m}{\Delta t \cdot w_o \cdot A_o} \cdot \left(\frac{2 \cdot \pi \cdot R \cdot T}{M_M}\right)^{1/2} \quad \text{(S5)}$$

where Δm is the mass of compound effused during the experimental time period Δt, M is the molar mass of the effusing vapor, R is the gas constant (8.3144598(48) J·mol^{-1}·K^{-1}), A_o is the area of the effusion orifice and w_o is the transmission probability factor, which is usually calculated by means of equation S6, where l is the length of the effusion orifice and r its radius:

$$w_o = \left\{1 + (3l / 8r)\right\}^{-1} \quad \text{(S6)}$$

In this technique only one effusion cell is used, with l = 0.05 mm and r = 0.600 mm, giving A_o = 1.1310 mm^2 and w_o = 0.970. The ln p = f (1 / T) results were fitted using the integrated form of the Clausius-Clapeyron equation:

$$\ln(p/p^*) = a - b/T \quad \text{(S7)}$$

where $b = \Delta_{cr}^{g} H_m^0(\langle T \rangle)/R$, and p^* = 1 Pa. The mean temperature, <*T*>, was taken as the average temperature concerning all the experimental data points, and $p(\langle T \rangle)$ is the pressure at that temperature, given by the ln $p = f(1/T)$ linear regression. $\Delta_{cr}^{g} S_m^0(\langle T \rangle)$ was then calculated according to the following equation:

$$\Delta_{cr}^{g} S_m^0(\langle T \rangle) = \Delta_{cr}^{g} S_m(\langle T \rangle, \langle p \rangle) + R \cdot \ln\left(\frac{\langle p \rangle}{10^5}\right) \quad \text{(S8)}$$

The vapor pressures of 1,3,5-triphenylbenzene were determined at 5 independent experiments. The experimental results are listed in Table S4; Table S5 lists the experimental results obtained from the Clausius-Clapeyron equation. The derived sublimation enthalpies and entropies for 1,3,5-triphenylbenzene, at θ = 298.15 K, are listed in table S6. The value of $\Delta_{sub}C_p^o$ = (-37.3 ± 8) $J \cdot K^{-1} \cdot mol^{-1}$ was used as the difference between the gas and solid phase heat capacity at 298.15 K.[S3-S6]

Table S4 Experimental vapor pressures of 1,3,5-triphenylbenzene (solid) obtained with the quartz crystal microbalance Knudsen effusion methodology.

T/K	*p*/Pa	Δ*p*/Pa	*T*/K	*p*/Pa	Δ*p*/Pa
		Experiment #01			
416.07	0.330	0.004	425.10	0.783	-0.003
419.08	0.440	0.001	428.10	1.040	-0.004
422.09	0.587	-0.002			
		Experiment #02			
407.04	0.129	-0.001	419.08	0.434	-0.005
410.05	0.175	-0.003	422.09	0.580	-0.009
413.06	0.237	-0.004	425.10	0.778	-0.008
416.07	0.321	-0.005	428.10	1.040	-0.004
		Experiment #03			
410.05	0.179	0.001	422.09	0.583	-0.006
413.06	0.241	0.001	425.10	0.779	-0.007
416.07	0.324	-0.002	428.10	1.043	-0.001
419.08	0.436	-0.003			
		Experiment #04			
405.54	0.111	0.001	420.58	0.505	-0.003
408.55	0.152	0.001	423.59	0.678	-0.002
411.56	0.206	-0.001	426.60	0.910	0.004
414.56	0.279	-0.001	427.60	1.004	0.008
417.57	0.377	-0.001			
		Experiment #05 (gravimetric)			
408.05	0.146	0.001	420.58	0.505	-0.003
410.55	0.187	0.001	423.09	0.647	-0.001
413.06	0.239	-0.002	425.60	0.826	0.002
415.57	0.310	0.001	428.10	1.070	0.026
418.08	0.399	0.001			

Table S5 Detailed results obtained for 1,3,5-triphenylbenzene, from the Clausius-Clapeyron equation.

a	b/K	r^2	$\langle T\rangle/K$	$p(\langle T\rangle)/Pa$	$\Delta_{\mathrm{sub}}H^{\circ}_{\mathrm{m}}\langle T\rangle$ / kJ·mol^{-1}	$\Delta_{\mathrm{sub}}S_{\mathrm{m}}\{\langle T\rangle; p(\langle T\rangle)\}$ /J·K^{-1}·mol^{-1}
Experiment #01						
39.8 ± 0.2	17007 ± 67	0.99995	422.09	0.589	141.4 ± 0.6	335.0 ± 1.3
Experiment #02						
40.4 ± 0.1	17275 ± 38	0.99997	417.57	0.374	143.6 ± 0.3	344.0 ± 0.8
Experiment #03						
40.0 ± 0.1	17130 ± 61	0.99994	419.08	0.437	142.4 ± 0.5	339.9 ± 1.2
Experiment #04						
40.4 ± 0.1	17285 ± 34	0.99997	414.56	0.280	143.7 ± 0.3	346.7 ± 0.7
Experiment #05 (gravimetric)						
40.5 ± 0.2	17308 ± 91	0.9998	418.08	0.399	143.9 ± 0.8	344.2 ± 1.8

Table S6 Standard molar enthalpies ($\Delta_{sub}H^o$), entropies ($\Delta_{sub}S^o$), and Gibbs energies ($\Delta_{sub}G^o$) of sublimation (sub), at θ = 298.15 K, for 1,3,5-triphenylbenzene.

Experiment	$\Delta_{sub}H^o$ kJ·mol^{-1}	$\Delta_{sub}S^o$ J·K^{-1}·mol^{-1}	$\Delta_{sub}G^o$ kJ·mol^{-1}
#01	146.0 ± 1.1	247.8 ± 3.1	72.1 ± 1.5
#02	148.1 ± 1.0	252.6 ± 2.8	72.8 ± 1.3
#03	146.9 ± 1.1	250.0 ± 3.0	72.4 ± 1.4
#04	148.1 ± 1.0	252.6 ± 2.7	72.7 ± 1.3
#05	148.4 ± 1.2	253.4 ± 3.3	72.8 ± 1.6
Final values	**147.5 ± 1.0**	**251.3 ± 2.3**	**72.6± 0.3**

4. Scanning Electron Microscopy

Thin films of mCP, CBP and TCB were produced by a vapor deposition procedure.[S3] All thin films were deposited under same experimental conditions: equilibrium vapor pressure of ≈ 0.3 Pa; mass flow rate at the substrate surface of ≈ 22 $ng \cdot cm^{-2} \cdot s^{-1}$; deposition time of 60 minutes; substrate temperature ≈ 293 K; mCP, CBP, and TCB were evaporated at 472, 545, and 573 K, respectively. The topography of the vapor-deposited thin films was investigated by scanning electron microscopy (SEM). SEM micrographs (top views) were acquired using a secondary electron detector (SE). Enlarged SEM images are depicted in Figures S7-S18.

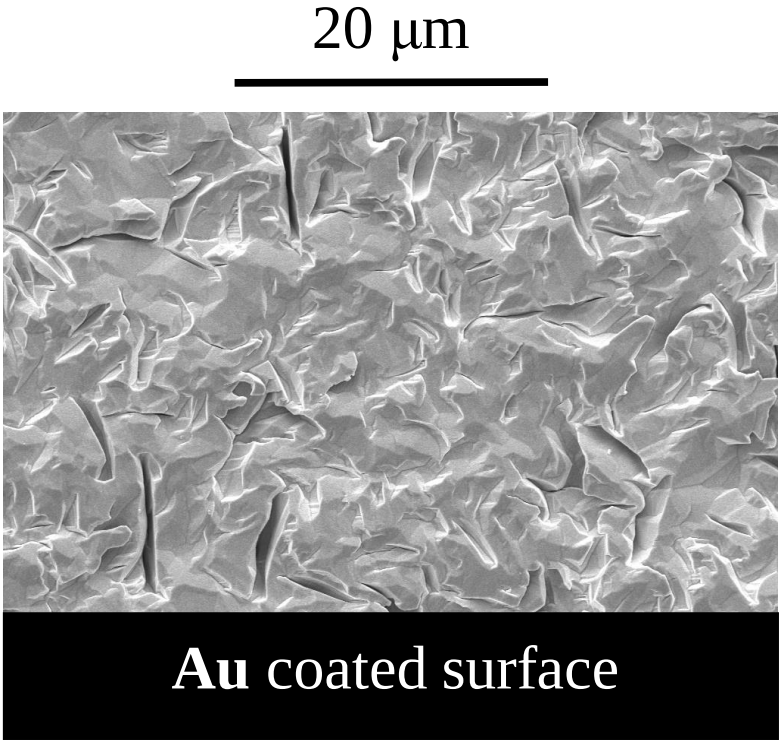

Fig. S7 Topographic image obtained by SEM of gold (Au) coated quartz crystal surface.

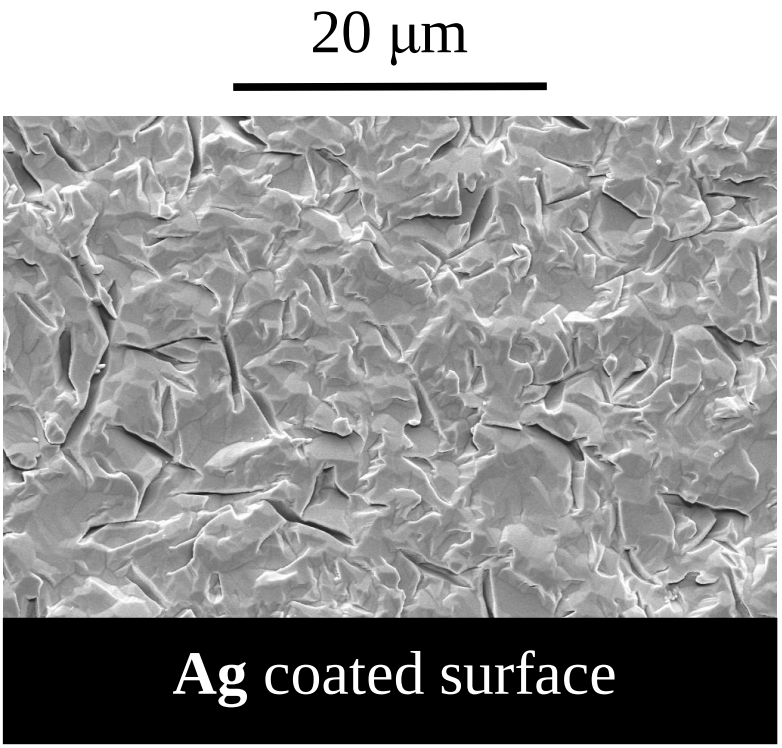

Fig. S8 Topographic image obtained by SEM of silver (Ag) coated quartz crystal surface.

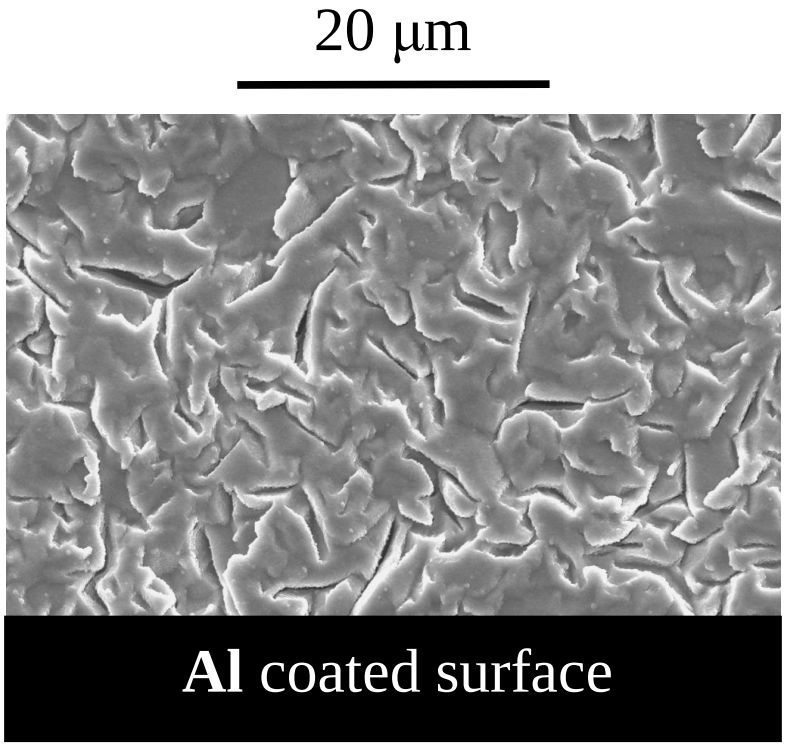

Fig. S9 Topographic image obtained by SEM of Aluminium (Al) coated quartz crystal surface.

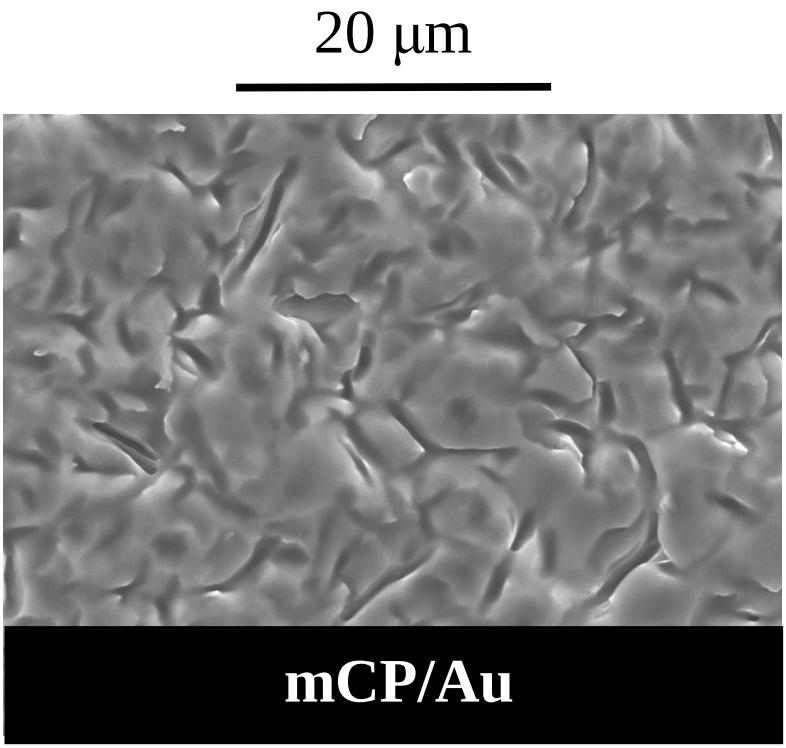

Fig. S10 Thin-film morphology of mCp deposited on Au coated quartz crystal surface.

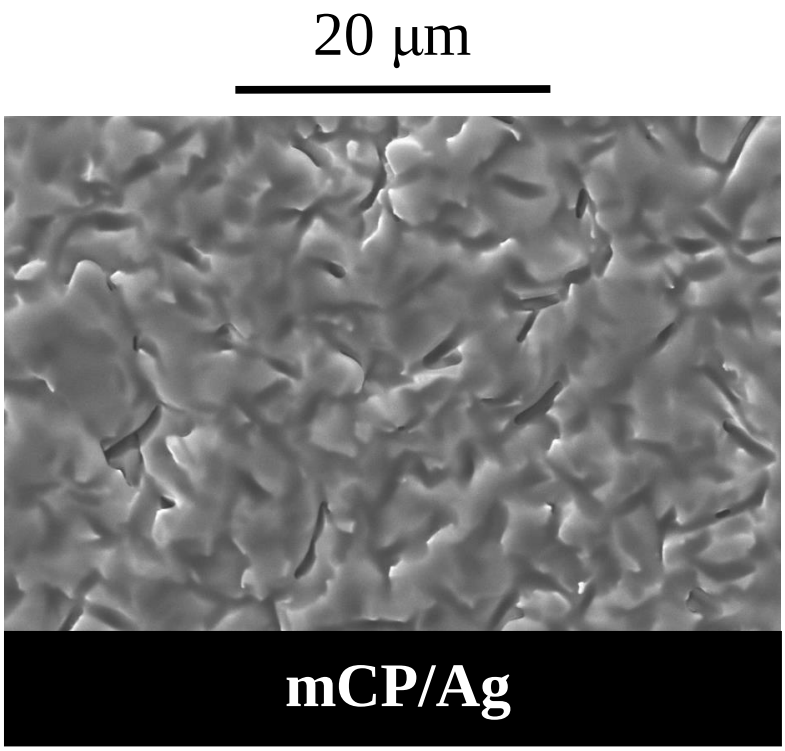

Fig. S11 Thin-film morphology of mCp deposited on Ag coated quartz crystal surface.

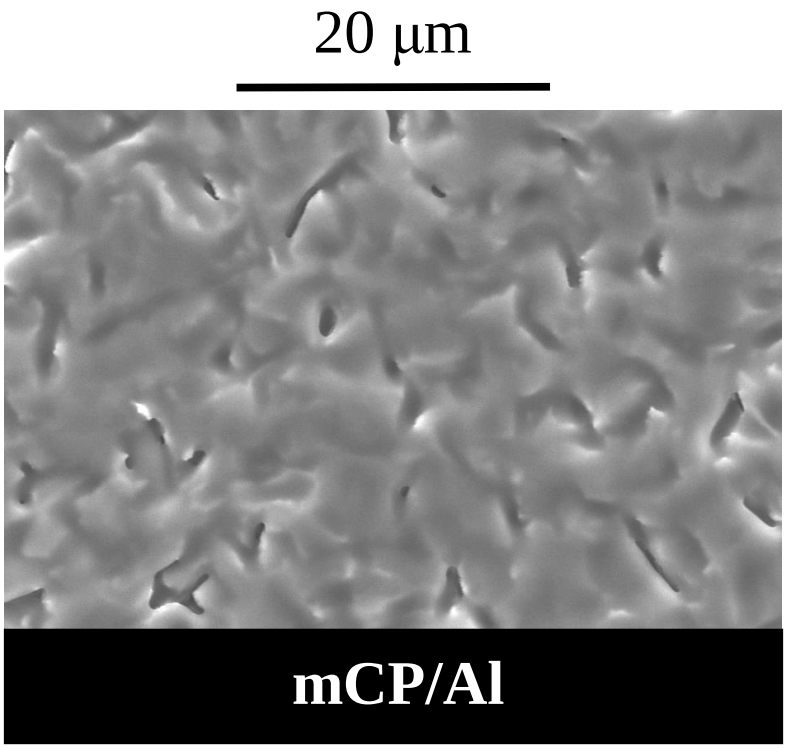

Fig. S12 Thin-film morphology of mCp deposited on Al coated quartz crystal surface.

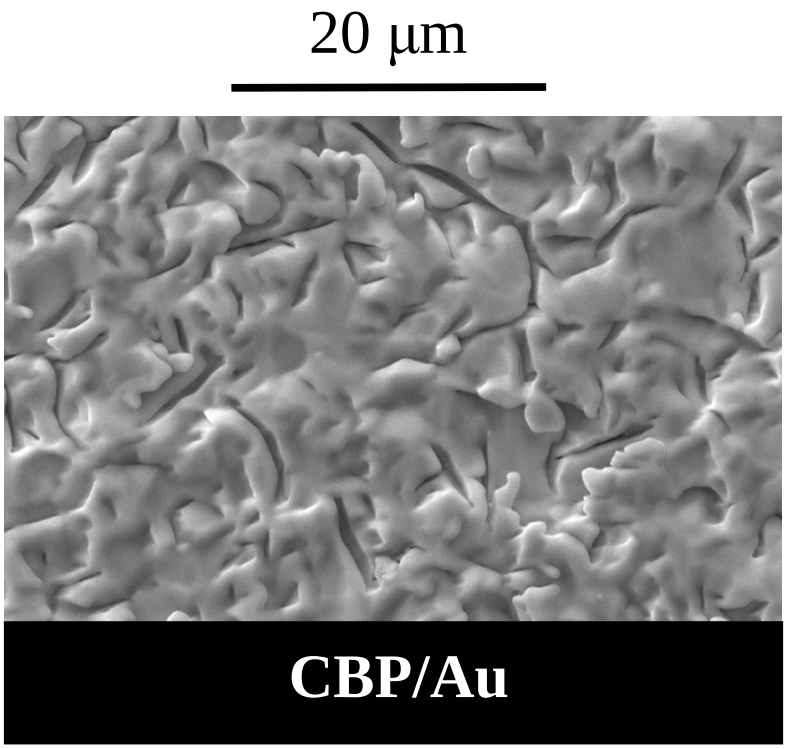

Fig. S13 Thin-film morphology of CBP deposited on Au coated quartz crystal surface.

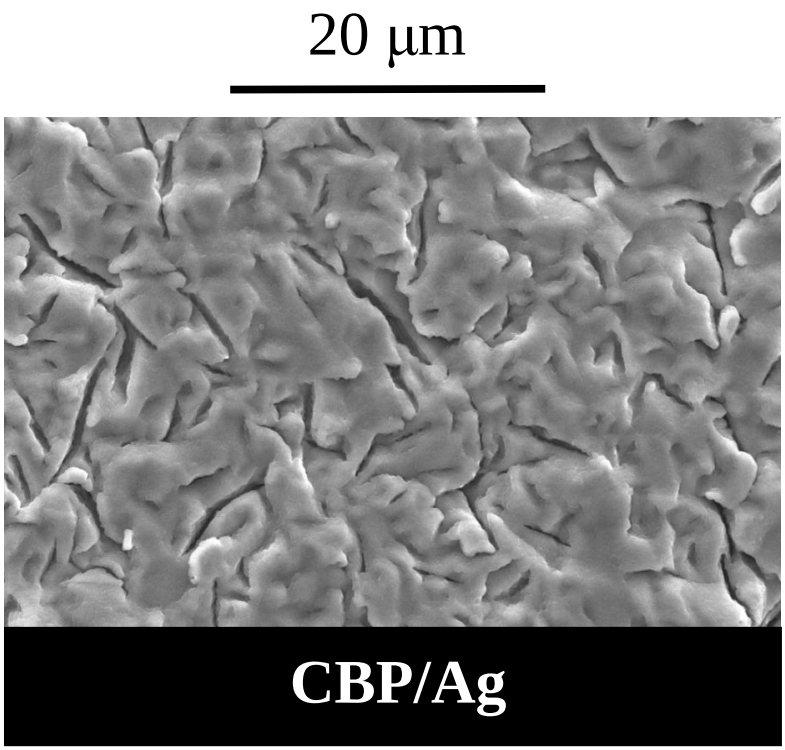

Fig. S14 Thin-film morphology of CBP deposited on Ag coated quartz crystal surface.

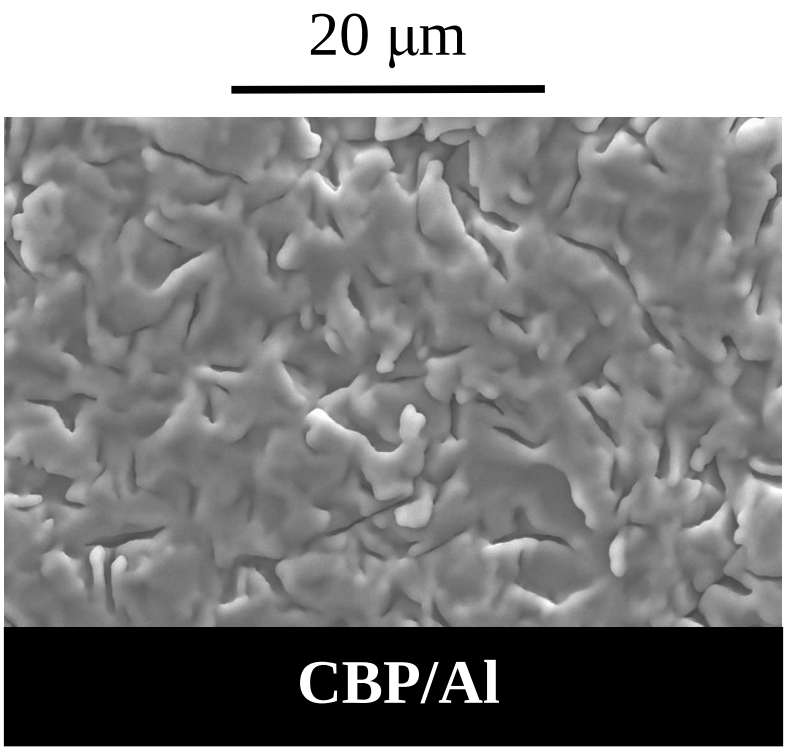

Fig. S15 Thin-film morphology of CBP deposited on Al coated quartz crystal surface.

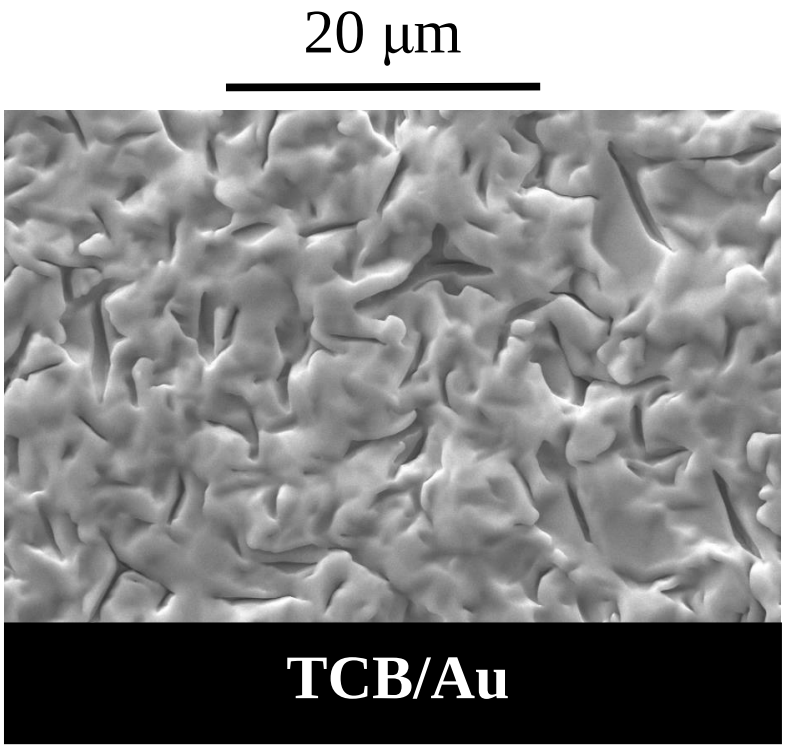

Fig. S16 Thin-film morphology of TCB deposited on Au coated quartz crystal surface.

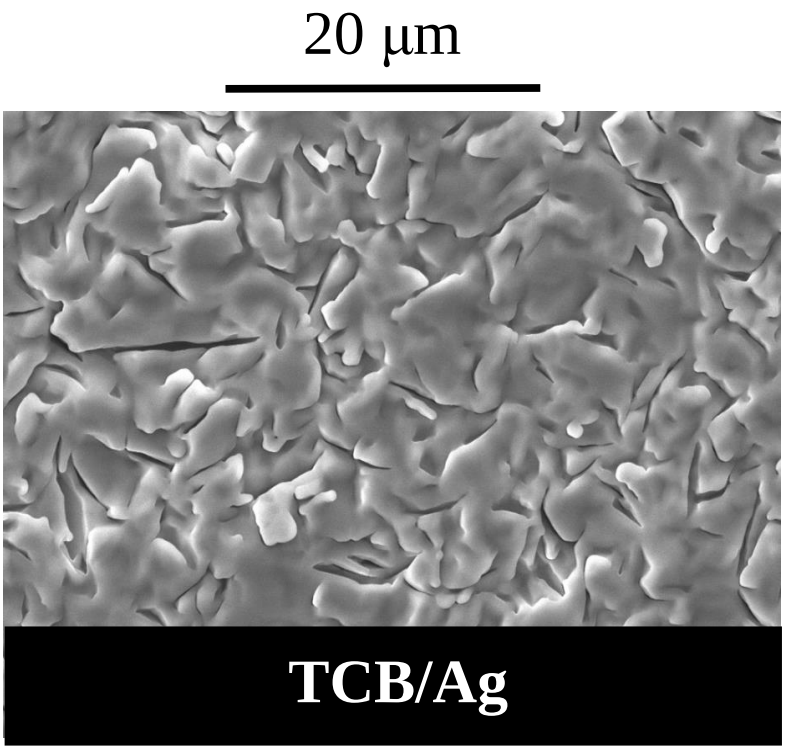

Fig. S17 Thin-film morphology of TCB deposited on Ag coated quartz crystal surface.

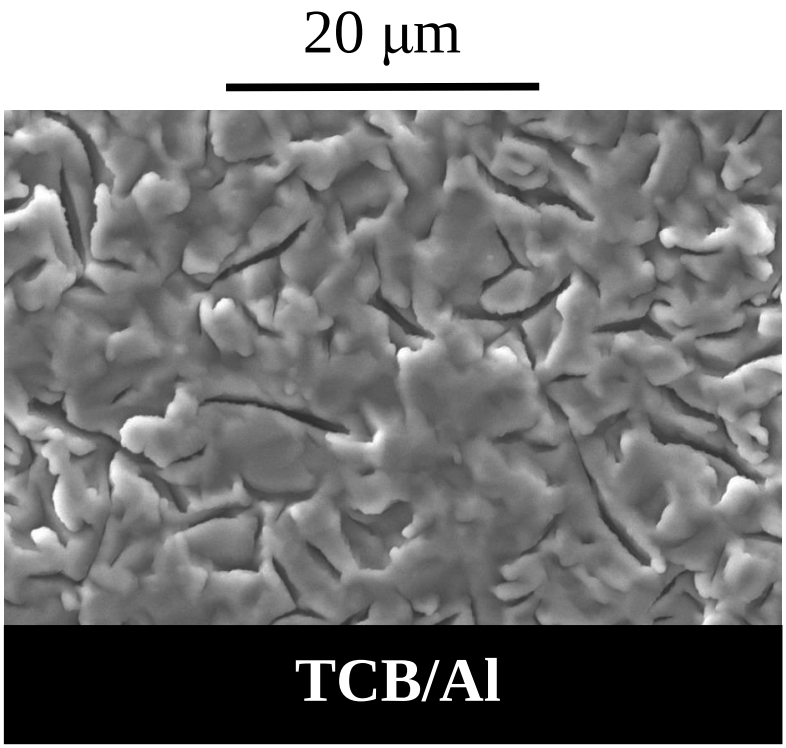

Fig. S18 Thin-film morphology of TCB deposited on Al coated quartz crystal surface.

References

(S1) R. Sabbah, A. Xu-wu, J. S. Chickos, M. L. Planas Leitão, M. V. Roux, L. A. Torres, *Thermochim. Acta*, 1999, **331**, 93−204.

(S2) M. V. Roux, M. Temprado, J. S. Chickos, Y. Nagano, *J. Phys. Chem. Ref. Data*, 2008, **37**, 1855−1996.

(S3) J. C. S. Costa, R. M. Rocha; I. C. M. Vaz; M. C. Torres, A. Mendes; L. M. N. B. F. Santos, *J. Chem. Eng. Data*, 2015, **60**, 3776−3791.

(S4) L. M. N. B. F. Santos, L. M. S. S. Lima, C. F. R. A. C. Lima, F. D. Magalhães, M. C. Torres, B. Schröder, M. A. V. Ribeiro da Silva, *J. Chem. Thermodyn.*, 2011, **43**, 834−843.

(S5) L. M. N. B. F. Santos, A. I. M. C. Lobo Ferreira, V. Stejfa, A. S. M. C. Rodrigues, M. A. A. Rocha, M. C. Torres, F. M. S. Tavares, F. S. Carpinteiro, *J. Chem. Thermodyn.*, 2018, **126**, 171−186.

(S6) M. A. V. Ribeiro da Silva, M. J. S. Monte, L. M. N. B. F. Santos, *J. Chem. Thermodyn.*, 2006, **38**, 778−787.

(S7) S. P. Verevkin, *J. Chem. Thermodyn.*, 1997, **29**, 1495−1501.

(S8) L. Malaspina, G. Bardi, R. Gigli, *J. Chem. Thermodyn.*, 1974, **6**, 1053−1064.

(S9) N. Wakayama, H. Inokuchi, *Bull. Chem. Soc. Jpn.*, 1967, **40**, 2267−2271.